Available online at www.sciencedirect.com
SCIENCE DIRECT®
Journal of Power Sources 140 (2005) 1–11
JOURNAL OF POWER SOURCES
www.elsevier.com/locate/jpowsour

Electroosmotic flow through polymer electrolyte membranes in PEM fuel cells

G. Karimi[1], X. Li*

Department of Mechanical Engineering, University of Waterloo, 200 University Avenue West, Waterloo, Ont., Canada N2L 3G1

Received 8 June 2004; accepted 12 August 2004
Available online 7 October 2004

Abstract

Water management is critically important for polymer electrolyte membrane fuel cells (PEMFC), and is complicated by the electroosmotic flow of water from anode to cathode through the polymer electrolyte membrane. In this study, electroosmotic flow in polymer electrolyte membranes is modeled incorporating the electrokinetic effect, and key parameters affecting the PEM fuel cell performance are identified. The governing Poisson–Boltzmann and the Navier–Stokes equations were solved numerically for a single membrane pore to determine the electroosmotic flow through the membrane over a wide range of geometrical and operating conditions. It was found that the electroosmotic drag coefficient, K_{Drag}, increases with the pore diameter. The membrane thickness has a significant effect on the electroosmotic flow. At constant cell voltage, the electroosmotic flow through thicker membranes (e.g. Nafion 117) is reduced because of the reduced electric field strength. The pressure difference required to stop electroosmotic flow is very large due to the extremely small pore diameters. In the presence of sulphuric acid, numerical results have revealed that the electroosmotic flow increases with the acid concentration.

Keywords: PEM fuel cell; Electroosmotic flow; Electroosmotic drag; Electrokinetic effect

1. Introduction

Polymer electrolyte membrane fuel cell (PEMFC) is one of the most promising candidates as zero emission power sources for both stationary and mobile applications. It is highly efficient and environmentally clean. During the PEMFC operations, the polymer electrolyte membrane provides the transport medium for the protons, generated during the anodic oxidation of the fuel, to migrate to the cathode and complete the electric and mass transport circuits. Therefore, high proton conductivity in the membrane is essential to achieve high performance in PEM fuel cells. The protonic current through the membrane, however, tends to drag water molecules along resulting in the water depletion at the anode side and water accumulation (hence flooding) at the cathode. This phenomenon, also called electroosmotic flow (or drag), increases the membrane resistance and reduces fuel cell performance [1,2].

The water content in the solid polymer electrolyte membrane is determined by the balance of water production at the cathode and its transport during the fuel cell operation. Fig. 1 depicts schematically the mechanisms of water transport in a PEM fuel cell. Water is carried into the fuel cell via the humidified gas streams entering gas diffusion electrodes. Some combination of water vapor and liquid water passes through each electrode to the electrode/membrane interface. Water crossing this interface assists in the hydration of the membrane. An additional source of water is the oxygen reduction reaction occurring at the cathode. Inside the membrane, water is transported in two ways: electroosmotic flow and back diffusion from cathode to anode. While both electroosmotic drag and water production due to oxygen reduction tend to create an excess of water near the cathode, back diffusion of water from cathode to anode tends to oppose the build-up of water and flatten the water concentration

* Corresponding author. Tel.: +1 519 888 4567x6843; fax: +1 519 888 6197.
[1] Permanent address: Shiraz University, Shiraz, Iran.
E-mail addresses: x6li@uwaterloo.ca (X. Li); gkarimi@engmail.uwaterloo.ca (G. Karimi).

0378-7753/$ – see front matter © 2004 Elsevier B.V. All rights reserved.
doi:10.1016/j.jpowsour.2004.08.018

Nomenclature

a	pore radius (m)
e	fundamental electronic charge (1.602×10^{-19} C)
E	electric field strength (V m^{-1})
E^*	non-dimensional term, Eq. (14)
F_E^*	non-dimensional electroosmotic force, Eq. (13)
F_P^*	non-dimensional pressure force, Eq. (13)
i	ion number in the electrolyte
Kn	Knudsen number
k_B	Boltzmann constant (1.381×10^{-23} J K^{-1})
K_{Drag}	electroosmotic drag coefficient
L	pore length (m)
M	molecular weight (kg mol^{-1})
M^*	non-dimensional term, Eq. (14)
n	iteration number
n_∞	bulk ionic number concentration (m^{-3})
N	local number concentration (m^{-3})
$\dot{N}$	molar flow rate (mol m^{-3} s^{-1})
N_A	Avogadro number (6.02×10^{23} particles mol^{-1})
P	pressure (Pa)
Q	volumetric flow rate (m^3 s^{-1})
r	pore radius (m)
r^*	non-dimensional pore radius
T	temperature (K)
u_{EO}	electroosmotic velocity (m s^{-1})
U	reference velocity (e.g. 1 mm s^{-1})
u^*	non-dimensional velocity
u_S^*	non-dimensional slip velocity
W	wall
z	valance of the dissolved ions

Greek letters

ϵ	dimensionless dielectric constant
ϵ_0	permittivity of vacuum (8.85×10^{-12} C^2 N^{-1} m^{-2})
κ	Debye–Huckle parameter (m^{-1})
μ	viscosity (Pa s)
ψ	potential (V)
ψ^*	non-dimensional potential
ρ	density (kg m^{-3})
ρ_e	net volumetric charge density (C m^{-3})
δ	lattice spacing (m)
Δ	difference
η	distance from the pore wall (Å)
ζ	zeta potential (V)

profile across the membrane. It is therefore very important to determine and manage the extent of the electroosmotic flow in the membrane to optimize the PEM fuel cell performance.

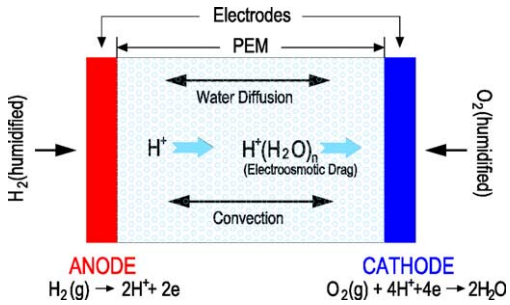

Fig. 1. Schematic of water transport and electroosmotic flow through the polymer electrolyte membrane in a PEM fuel cell.

The electroosmotic drag coefficient, K_{Drag}, defined as the number of water molecules transferred through the membrane per proton in the absence of other water transport mechanisms, has been measured by a variety of techniques. The measured value of this coefficient for Nafion, the most commonly used membrane, however, exhibits a wide scatter. LaConti et al. [3] measured the transferred water volume using capillary tubes. They reported a linear increase in K_{Drag} from 0 (in the dry state) to 4–5 (in the fully hydrated state) for Nafion membranes with equivalent weights of 1150–1275 and found no temperature dependence. Zawodzinski et al. [1] used a similar method and obtained K_{Drag} between 0.9 and 2.5 for partially and fully hydrated Nafion 117 membrane at 300 K, respectively. Fuller and Newman [4] measured electroosmotic drag for Nafion 117 in a H_2O concentration cell. They reported $K_{Drag} \approx 1.4$ for hydrated membrane and a decrease to $K_{Drag} = 0$ for the dry membrane at 25 °C. From the same kind of measurement, Zawodzinski et al. [2] later found $K_{Drag} = 1$ for vapor-equilibrated membranes over a wide range of water content and almost independent of the membrane microstructure. In fact, this coefficient would best represent the macroscopic phenomenon of electroosmotic drag in an operating PEM fuel cell, since the majority of the water molecules in the membrane are in the form of vapor at the fuel cell operating conditions. Xie and Okada [5] measured $K_{Drag} = 2.6$ for a fully hydrated membrane using the streaming potential. Recently, Ren et al. [6] presented a method of measuring electroosmotic drag in a direct methanol fuel cell and obtained, for a fully hydrated membrane, an increase of K_{Drag} as a function of temperature from 1.9 at 15 °C to 5.1 at 130 °C. The wide range of scatter in the reported K_{Drag} clearly shows the sensitivity and difficulties involved with the experimental techniques.

The PEM electroosmotic driven flow in general, and the electroosmotic drag in particular, can also be investigated with the knowledge of the pore geometry and electrokinetic effect. It is therefore the aim of this study to develop a model that describes, under steady-state conditions, the electroosmotic flow in an operating fuel cell using the fundamental physical mechanisms. The formulation is from a macroscopic point of view, but with sufficient incorporation of the nanoscopic information, although it may be much simplified, such that the resulting model has sufficient pre-

dictive capability with acceptable accuracy for macroscopic engineering application. Therefore, it is not interested in including all the fine features of the nanoscopic or molecular level mechanisms of the proton transport processes. To this end, the Poisson–Boltzmann and the Navier–Stokes equations were solved numerically to investigate the electroosmotic flow in a simplified PEM pore configuration over a wide range of geometrical and operating conditions.

2. Model formulation

2.1. The physical problem

Perfluorinated sulphonic membranes, such as Nafion, are the ionomeric materials typically used in PEM fuel cells. The study of water and ions transport in polymer electrolyte membranes requires extensive knowledge of the membrane morphology, water sorption thermodynamics and proton distribution in the membrane, interactions between the protons and the membrane, and proton transport in aqueous solution. A great number of experimental techniques have been applied in an effort to understand the morphology and ion distribution of polymer electrolyte membranes and the correlation of these two properties. Some of these techniques include small and wide angle X-ray scattering [7,9], dielectric relaxation [10], dielectric spectroscopy [11], electron microscopy [12], and AC impedance investigations [13], to quote a few. Despite the substantial work conducted for characterization of polymer electrolyte membranes, a fundamental understanding of the mechanisms of proton and water transport is not fully understood [14]. This is largely due to the very inhomogeneous nature of these membranes when hydrated. However, majority of these studies consider polymer electrolyte membrane as being made of three microphase-separated regions as illustrated in Fig. 2. According to these models, region A consists of hydrophobic fluorocarbon backbone material. The ion-cluster regions, C, generally described as pores or aqueous solution environments, with sulphonate groups ($-SO_3^-$) as fixed-charge sites and movable ions (usually H^+ for acidic membranes) as counterions. The interconnecting region B is an amorphous hydrophobic region of lower ionic content. The hydrophilic ion clusters C and region B are responsible for ionic conduction. A network of these hydrophilic clusters of the size 50–60 Å is cross-connected with other hydrophilic channels of smaller diameters 10–20 Å [8].

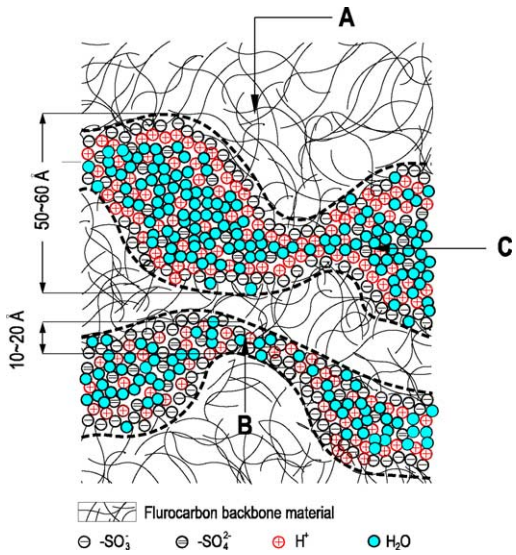

Fig. 2. Nafion cluster network model [7,8].

A number of physical models have also been developed to identify the mechanisms of water and ion transport in the ionomer membranes. The hydrodynamic model approach [15], solubility and transport models [16], partition coefficient model [17,18], and random network model of a microporous polymer electrolyte membrane [19] are only a few examples. These models do not represent the true morphological features associated with the ionomer membranes, and rely on the input parameters. As a result, their predictions often deviate from the experimental measurements.

Molecular theoretical studies [20,21] directed towards understanding these remarkable properties of ionomer membranes are limited for several reasons. Polar-solvent environments profoundly affect charge transport processes like proton transfer, where collective solvent effects, including orientational polarization, require consideration of large molecular ensembles in computer simulations. Proton motion exhibits quantum mechanical behavior such as zero-point energy constraints and tunneling, requiring quantum mechanical treatment that is computationally challenging and expensive in multi-body systems.

On the other hand, the proton transport through the membrane electrolyte has been conventionally modeled by the phenomenological Ohm's law in most of engineering-oriented calculations for operating fuel cells [22]. This macro-homogeneous approach does not offer any fundamental insight on the mechanism of actual proton transport processes at the molecular level. The present model envisions the electroosmotic drag phenomenon from another perspective. The hydrophilic tortuous electrolyte regions within the membrane are considered as continuous, parallel conduction pathways with average diameters ranging from 20 to 80 Å, perpendicular to the membrane surface with uniform sulphonic ions fixed at the wall resulting in an equipotential surface. The physical and electrochemical properties (with the exception of electrolyte permittivity) are assumed to be constant and independent of the position. This approach is advantageous because it is physically sound, simple, and requires no experimental data. As a result, it can be used for parametric study and provides some design and optimization rules without going into the detailed molecular level transport phenomena.

The presence of the negative sulphonic charge on the wall results in the formation of a diffuse layer of counterions (e.g. protons in the present case) where the concentration near the

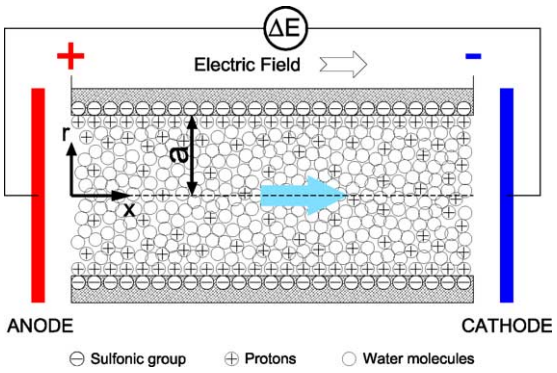

Fig. 3. Electroosmotic flow of water in a membrane pore of a PEM fuel cell.

sulphonic wall is at the highest and decreases gradually with distance until it reaches equilibrium [23]. The resulting electric potential is therefore minimum at the wall and gradually increases towards an equilibrium level as the concentration of protons approaches the bulk concentration at farther distances.

If an electric field is applied across the membrane, as in an operating fuel cell, an electrokinetic body force is exerted on the charged analytes (e.g. free H^+ ions not interacting with SO_3^-). The protons will then move in the narrow hydrophilic pores under the influence of the applied electric field, taking with them the hydrating water molecules, and resulting in an electroosmotic flow as illustrated in Fig. 3. The fluid movement is carried through to the rest of the fluid in the pores by viscous forces. It should be pointed out that the electric potential (or field) across the membrane, as shown in Fig. 3, is after considering the effect of the electric double layers near the electrode and the membrane electrolyte interface [24].

2.2. The charge distributions

The electric potential distribution existing in the charged analytes flowing inside a membrane pore shown in Fig. 3 is due to the presence of diffuse layer in a cylindrical pore; it can be related to the local volumetric net charge density of the electrolyte, ρ_e, using theory of the electrostatics [25]:

$$\nabla \cdot (\epsilon \nabla \psi) = -\frac{\rho_e}{\epsilon_0} \tag{1}$$

where ϵ is the dimensionless dielectric constant of the electrolyte, ψ is the electrostatic potential, and ϵ_0 is the permittivity of vacuum. The dielectric constant of the electrolyte varies as a function of the radial distance from the pore wall due to the change in the orientations of the water molecules. A dielectric saturation model was developed by Paddison and Paul [26] for fully hydrated Nafion membranes. According to this model, dielectric constant remains that of bulk water for distances of at least 12 Å from the wall, but begins to fall sharply as the arrays of $–SO_3^-$ fixed sites are approached. Based on their model, variations of dielectric constant as a function of the distance from the pore wall, η, can be approximated mathematically as:

$$\epsilon = \begin{cases} 17 & \eta \le 7.8\,\text{Å} \\ 17 + 23.7(\eta - 7.8) & 7.8 < \eta \le 10.5\,\text{Å} \\ 81 & \eta > 10.5\,\text{Å} \end{cases} \tag{2}$$

The net charge density can be expressed in terms of the Boltzmann distribution as [25]:

$$\rho_e = \sum z_i e n_{i,\infty} \exp\left(\frac{-z_i e}{k_B T}\psi\right) \tag{3}$$

where z_i is the valence of the dissolved ions, $n_{i,\infty}$ is the ionic number concentration in the bulk solution, e is the fundamental electronic charge, k_B is Boltzmann's constant, and T is the absolute temperature.

Eq. (3) can be simplified for the proton-conducting membrane used in PEM fuel cells where only counterions (H^+, $z = +1$) are present:

$$\rho_e = z e n_\infty \exp\left(\frac{-ze}{k_B T}\psi\right) \tag{4}$$

Substitution of Eq. (4)into Eq. (1) and transforming it into non-dimensional form results in the Poisson–Boltzmann equation as follows:

$$\frac{1}{r^*}\frac{d}{dr^*}\left(r^*\frac{d\psi^*}{dr^*}\right) = -\frac{1}{2}(\kappa_1 a)^2 \exp(-\psi^*) \tag{5}$$

The non-dimensional variables are defined as:

$$\psi^* = \frac{\psi}{(k_B T)/(ze)} \quad \text{and} \quad r^* = \frac{r}{a} \tag{6}$$

where r is the radial distance and a is the pore radius.

The so-called Debye–Huckle parameter, κ_1, which is a measure of the diffuse layer thickness, is defined as [27]:

$$\kappa_1 = \left(\frac{2n_\infty z^2 e^2}{\epsilon\epsilon_0 k_B T}\right)^{1/2} \tag{7}$$

Eq. (5) is subject to the following boundary conditions:

$$\text{at } r^* = 0, \quad \frac{d\psi^*}{dr^*} = 0; \quad \text{and}$$

$$r^* = 1, \quad \psi^* = \frac{\psi_W}{(k_B T)/(ze)} = \psi_W^* \tag{8}$$

The potential at the pore wall, ψ_W, which is also the boundary of the fluid flow problem, is called zeta potential, ζ. This potential is typically determined empirically from electroosmotic or streaming potential flow measurements [27].

2.3. The velocity distribution

The electroosmotic-induced flow can be obtained with the knowledge of the liquid velocity distribution. With the pore sizes in the order of nanometers, the Reynolds number is very small and the entry length effects can be neglected such that the axial velocity would be a function of radius (r) only.

However, the minute pore geometry may not hold enough number of molecules to satisfy completely the concept of continuum. The corresponding Knudsen (Kn) number can be calculated from:

$$Kn = \frac{\delta}{a} \tag{9}$$

where the lattice spacing, δ, is about 3 Å for water [28]. For an average pore size of 50 Å, the Knudsen number is about 0.06 and a slip flow regime is expected to exist in the pore. In the absence of thermal creep, the dimensionless slip velocity at the pore wall is calculated as:

$$u_S^* = Kn \frac{\partial u_s^*}{\partial n} \tag{10}$$

where n and subscript s stand for the outward normal (unit) vector and the tangential (unit) vector [29].

For the pore wall negatively charged, the electroosmotic flow will be in the direction towards the cathode as illustrated in Fig. 3. The body force per unit volume created by electric field acting on the charged particles is given by $F_E = \rho_e E$, where E is the electric field strength. The Navier–Stokes equations for a Newtonian laminar liquid flow with constant density, ρ, and viscosity, μ, in a horizontal cylindrical capillary under the influence of both an external electric force and pressure gradient can be expressed as [25]:

$$\mu \nabla^2 u - \nabla p + \rho_e E = 0 \tag{11}$$

representing the balance among the net viscous force, pressure force, and electric force acting on the fluid particles for the steady flow under consideration.

Eq. (11) can be non-dimensionalized as:

$$\frac{1}{r^*} \frac{\mathrm{d}}{\mathrm{d}r^*} \left(r^* \frac{\mathrm{d}u^*}{\mathrm{d}r^*} \right) + F_P^* + F_E^* = 0 \tag{12}$$

where u^* is the liquid velocity normalized with some reference velocity, U, considered as $1\,\mathrm{mm\,s^{-1}}$ throughout this work. F_P^* and F_E^* are non-dimensional pressure and electroosmotic body forces, respectively, defined as:

$$F_P^* = \frac{\Delta P a^2}{\mu U}, \qquad F_E^* = M^* \rho_e^* E^* \tag{13}$$

and

$$M^* = \frac{z e n_\infty \zeta a^2}{\mu U L}, \qquad E^* = \frac{E L}{\zeta},$$

$$\rho_e^* = \frac{\rho_e}{z e n_\infty} = \exp(-\psi^*) \tag{14}$$

where ΔP represents the pressure difference between the anode and cathode ends of the pore and L is the capillary length. The dimensionless group, M^*, is the ratio of the electric to viscous forces per unit volume. Eq. (12) shows that pore hydrodynamics is influenced by two driving forces: pressure difference across the membrane and the electric force acting on the charge carriers.

Eq. (12) is subject to the following boundary conditions:

$$\text{at } r^* = 0, \quad \frac{\mathrm{d}u^*}{\mathrm{d}r^*} = 0; \quad \text{and}$$

$$r^* = 1, \quad u^* = u_S^* \text{ (slip velocity)} \tag{15}$$

3. Solution method

There is no exact solution for the non-linear Poisson–Boltzmann equation, Eq. (5). A finite volume scheme with variable cell spacing was developed to discretize the equation. To facilitate convergence, the exponential term has been linearized as follows:

$$\exp(-\psi_{n+1}^*) = \exp(-\psi_n^*) - \exp(-\psi_n^*)\left(\psi_{n+1}^* - \psi_n^*\right) \tag{16}$$

where n refers to the iteration number.

The resulting system of algebraic equations was solved using the Gauss–Seidel iterative technique. Totally, 500 control volumes were created. The grid spacings were reduced successively by 5% to condense the control volume sizes in the region near the wall, where the electroosmotic effect is significant. The calculated electric potential distribution is then substituted into the momentum equation, Eq. (12), which is also solved numerically to obtain the flow distribution. A tridiagonal matrix algorithm (TDMA) was implemented to obtain pore velocity profiles and the electroosmotic drag coefficient in the capillary pores.

4. Results and discussions

Non-dimensional potential and Navier–Stokes equations were solved simultaneously to obtain the electroosmotic flow and to identify its flow characteristics in a PEM pore structure under a variety of design and operating conditions. All of the simulations are based on fully hydrated Nafion membranes under the condition that the water content of the membrane on the anode side is sufficiently high to replenish the water and maintain the membrane hydration. The membrane thickness is considered to be inflated by 30% to account for the hydration. The parameters studied and the cell physical properties are summarized in Table 1.

Table 1
Parameters and properties used in the present PEM simulations

Quantity	Value
Cell temperature	80 °C
Pore water viscosity	$3.6 \times 10^{-4}\,\mathrm{kg\,m^{-1}\,s^{-1}}$
Pore water density	$980\,\mathrm{kg\,m^{-3}}$
Cell voltage	0.70 V
Fixed charge site concentration [31]	$1.2 \times 10^{-3}\,\mathrm{mol\,cm^{-3}}$
Wet membrane thickness[a]	
Nafion 117	2.31×10^{-4} m
Nafion 115	1.65×10^{-4} m
Nafion 112	6.60×10^{-5} m

[a] Inflated thickness.

4.1. Estimation of ζ potential

In order to solve the governing equations, one needs to know the wall potential (ζ potential). To the best knowledge of the authors, this quantity has not been yet reported for the membrane in PEM fuel cell under operating conditions. Therefore, in the first set of calculations, the ζ potential was varied over a reasonable range (from -400 to -100 mV) and the resulting electroosmotic drag coefficients were compared with the already reported values in the literature.

Fig. 4a depicts the variation of the non-dimensional charge density, ρ_e^*, as a function of the non-dimensional pore radius, r^*, for three different ζ potential values and zero pressure difference between the anode and cathode ends. As expected, the sulphonic wall attracts free protons creating a large charge density at the boundary. The charge density decreases rapidly away from the wall and levels off at the pore center. The resulting non-dimensional potential and velocity distribution are shown in Fig. 4b and c, respectively. As seen in Fig. 4b, the electric potential has a minimum at the wall $r^* = 1$ (i.e. the ζ potential), and increases rapidly towards the pore center. The effect of the cell electric field is thus maximum in the near wall region where ρ_e^* is at the highest. From Fig. 4c, it is seen that a non-zero velocity (u_S^*) exists at the wall which increases slowly in the direction of the pore centerline such that a plug-type flow distribution prevails in the pore. The larger the ζ potential (absolute value), the stronger the driving forces (by increasing ρ_e^*), thus the larger the electroosmotic flow in the pore.

The volumetric flow rate arising from the electroosmotic flow in the capillary pore was calculated by integrating the velocity distribution across the pore area. Fig. 5a displays the variation of the flow rate as a function of the ζ potential. The electroosmotic drag coefficient can then be calculated from:

$$K_{\text{Drag}} = \frac{\dot{N}_{H_2O}}{\dot{N}_{H^+}} = \left(\frac{\rho}{M}\right)_{\text{Water}} \frac{N_A \int_0^a u_{EO}(r) r \, dr}{\int_0^a N_{H^+}(r) u_{EO}(r) r \, dr} \qquad (17)$$

where N_A is the Avogadro number, M is the molecular weight, N_{H^+} is the number density for protons, and u_{EO} is the velocity distribution due to the electroosmotic flow.

The variation of K_{Drag} as a function of ζ potential is shown in Fig. 5b. As seen from this figure, the most reasonable ζ potential is the one giving rise to $K_{\text{Drag}} = 1$, comparable with the previous studies summarized in Section 1. Therefore, the corresponding value of $\zeta = -0.327$ V is taken for the current parametric study calculations which are presented in the following sections.

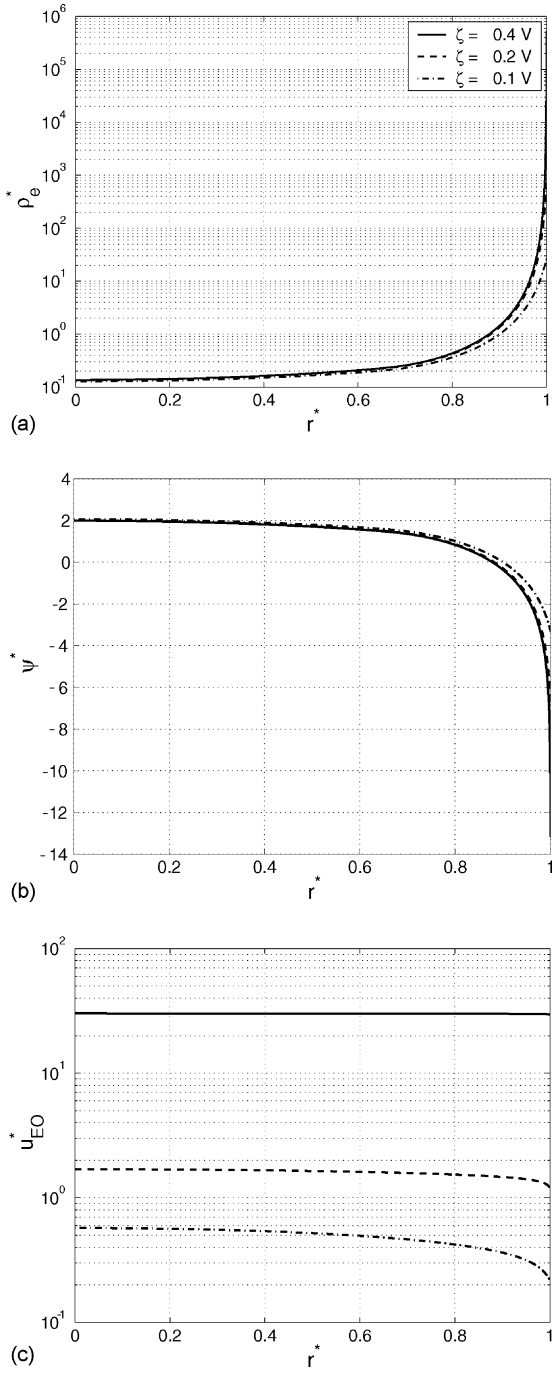

Fig. 4. Effect of zeta potential on the distribution of (a) the charge density, (b) the potential, and (c) the resulting electroosmotic velocity through the fully hydrated Nafion 117 membrane with the parameter values: $\psi_W^* = (-13.15, -6.57, -3.29)$, $P^* = 0$, $M^* = (-3.48, -1.74, -0.87)$, and $E^* = (-1.75, -3.5, -7.0)$.

4.2. Effect of pore diameter

There exists a pore size distribution in the Nafion membrane. Therefore, it would be useful to investigate the effect of pore diameter on the electroosmotic flow. Theoretically, pore diameter not only affects the diffuse layer thickness ($\kappa_1 a$ in Eq. (5)), but also influences the strength of the viscous forces (M^*) in Eq. (14). Fig. 6a shows that the larger the pore diameter, the lesser the charge density becomes towards the pore centerline. Also, the larger source term in Eq. (5) results in a larger potential at the pore centerline, as shown in Fig. 6b. The larger diameter further enhances electroosmot-

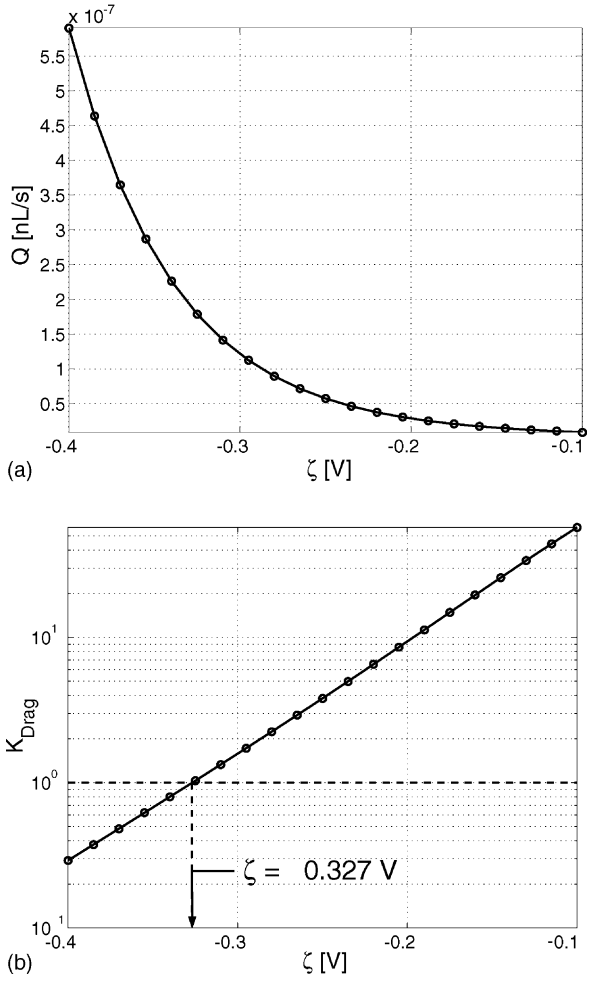

Fig. 5. The variation of (a) a single pore flow throughput and (b) the electroosmotic drag coefficient as a function of the ζ potential for the fully hydrated Nafion 117 membrane.

ically induced flow velocity in the pore structure, evident in Fig. 6c.

With no pressure difference, Fig. 7a shows how the electroosmotic flow through a single pore increases non-linearly with the pore size. Variation of the K_{Drag} with the pore size given in Fig. 7b reveals that this parameter is almost linearly changing with the pore diameter.

4.3. Effect of electric field strength

Both membrane thickness and the cell voltage affect the electric field strength across the electrolyte membrane. Although the potential distribution is unaffected, the electroosmotic velocity increases linearly with E (Eq. (14)). This linear dependency has been experimentally observed for electric field strengths of up to $3 \times 10^7\ \mathrm{V\,m^{-1}}$ [30].

If the cell voltage remains constant, F_E^* will inversely decrease with the membrane thickness resulting in a significantly lower electroosmotic flow (or higher water content) for thicker membranes such as Nafion 117 as shown in Fig. 8.

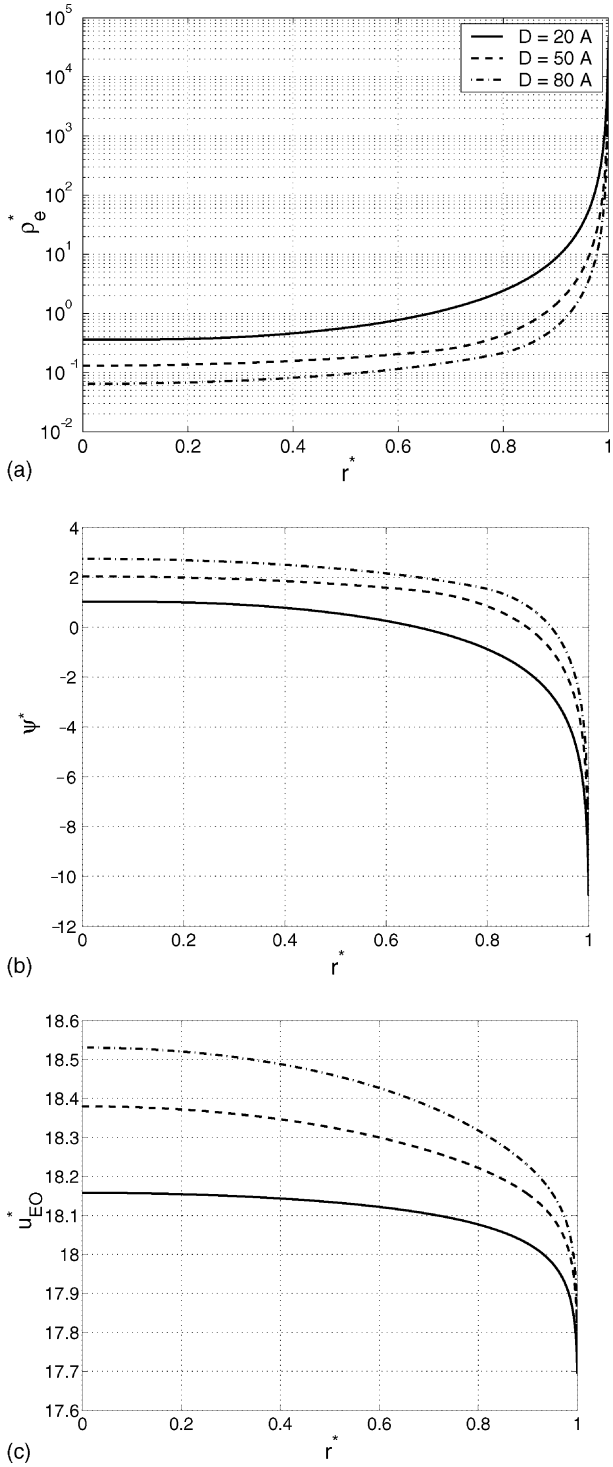

Fig. 6. Effect of pore diameter on the distribution of (a) the charge density, (b) the potential, and (c) the resulting electroosmotic velocity for the fully hydrated Nafion 117 membrane with the parameter values: $\psi_{\mathrm{W}}^* = -10.75$, $P^* = 0$, $M^* = (-0.46, -2.84, -7.28)$, and $E^* = -2.14$.

However, this could be balanced with the lower back diffusion and higher ohmic resistance usually involved with thicker membranes. On the other hand, K_{Drag} is unaltered as the potential distribution is unaffected by the membrane thickness.

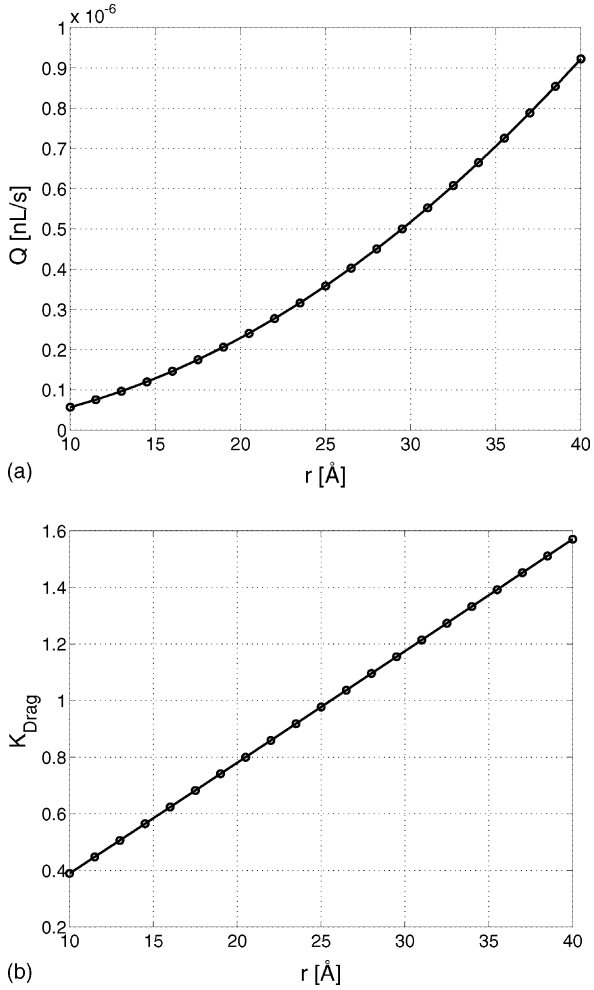

Fig. 7. The variation of (a) a single pore flow throughput and (b) the electroosmotic drag coefficient as a function of the pore diameter for the fully hydrated Nafion 117 membrane.

4.4. Effect of pressure differential

Net water transport in the membrane arises from three mechanisms: electroosmotic drag, convection, and diffusion. The effect of the first two mechanisms on the membrane conductivity is shown in Eq. (12). The momentum equation is linear and one can decompose the velocity field into two parts:

$$u^* = u^*_{\mathrm{EO}} + u^*_{\Delta P} \tag{18}$$

where u^*_{EO} and $u^*_{\Delta P}$ correspond to the non-dimensional electroosmotic and pressure-driven capillary flow velocities, respectively.

If the electroosmotic flow is to be stopped exclusively by applying a pressure difference across the membrane, one may use the Poiseuille equation for fully developed flow in circular tubes to estimate the required pressure as follows:

$$\Delta P = \frac{8\mu L Q}{\pi a^4} \tag{19}$$

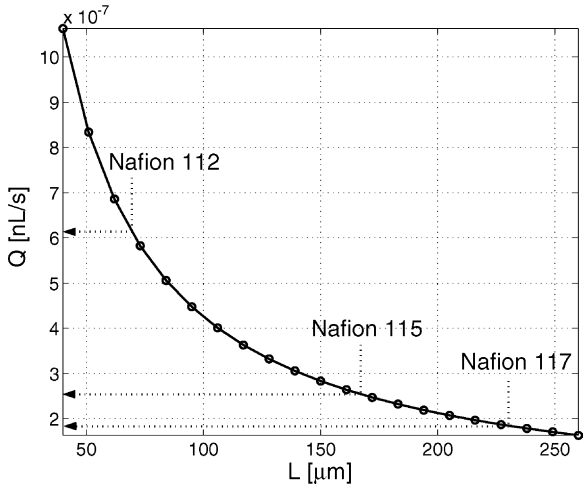

Fig. 8. The variation of electroosmotic flow as a function of the PEM thickness, L, for the fully hydrated Nafion membrane with the parameter values: $\psi^*_{\mathrm{W}} = -10.75$; $P^* = 0$; $M^* = -9.96$ for Nafion 112, -3.98 for Nafion 115, and -2.84 for Nafion 117.

With the electroosmotic flow rates determined, the ΔPs calculated from Eq. (19) are extremely large and impractical to apply. This is due to the very small pore diameters in the membrane. Fig. 9 indicates that a pressure difference of about 19,000 atm is required to stop completely the electroosmotic flow from anode to cathode in Nafion 117 membrane. However, in practice, application of a few atm pressure differences has provided a better cell performance due to reduced drying on the anode side of the membrane.

4.5. Effect of sulphuric acid

Preparation of polymer electrolyte membrane is a key factor for the fuel cell performance. During the preparation, the solid electrolyte integrated with the catalyst layers and elec-

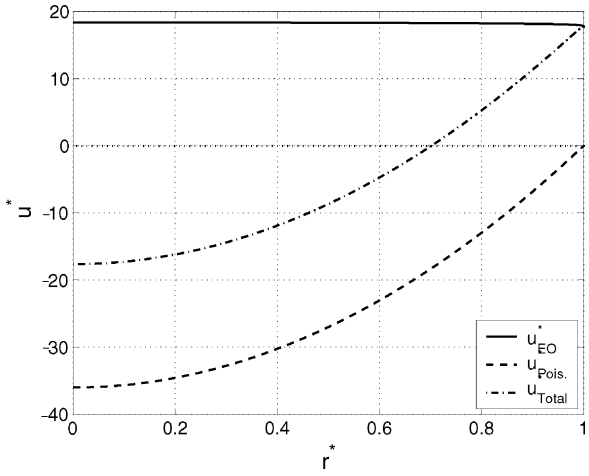

Fig. 9. Counterbalance of electroosmotic and pressure-driven flows in a fully hydrated, fully developed Nafion membrane pore with the parameter values: $\psi^*_{\mathrm{W}} = -10.75$, $P^* = -144$, $M^* = -2.84$, and $E^* = -2.14$.

trodes is cleaned by immersing in boiling hydrogen peroxide solution. This is followed by boiling it in sulphuric acid to ensure a full protonation of the sulphonate groups. The process is completed by rinsing the membrane in boiling de-ionized water to remove any remaining acid. It is therefore possible for some sulphuric acid traces to escape the rinsing process. In some applications, sulphuric acid is intentionally added to the membrane to enhance its conductivity properties. In this section, the effect of the presence of sulphuric acid in the membrane on the electroosmotic flow is investigated.

Ionization of sulphuric acid in the membrane modifies the Poisson–Boltzmann equation, Eq. (5), by influencing the charge density distribution. With extra H^+ and $SO_4{}^{2-}$ ions present, the non-dimensional net charge density, ρ_e^*, becomes:

$$\rho_e^* = \exp(-\psi^*) + 2\frac{n_{2,\infty}}{n_\infty}\left[\exp(-\psi^*) - \exp(2\psi^*)\right] \qquad (20)$$

where $n_{2,\infty}$ is the sulphuric acid bulk number concentration. The contributions from the acid, H^+ and $SO_4{}^{2-}$ ions, are represented by the second and third terms in Eq. (20), respectively. The modified Poisson–Boltzmann equation becomes:

$$\frac{1}{r^*}\frac{\mathrm{d}}{\mathrm{d}r^*}\left(r^*\frac{\mathrm{d}\psi^*}{\mathrm{d}r^*}\right) = -\frac{1}{2}(\kappa_1 a)^2\exp(-\psi^*) + (\kappa_2 a)^2\left[\exp(2\psi^*) - \exp(-\psi^*)\right] \qquad (21)$$

where κ_2 is the same as κ_1 except n_∞ replaced by $n_{2,\infty}$. The change in the potential distribution due to the presence of sulphuric acid also changes the source term in the momentum equation (e.g. F_E^* in Eq. (12)) and modifies the electroosmotic flow distribution in the membrane. Due to the lack of experimental or theoretical data, it is assumed that acid presence does not influence the ζ potential appreciably.

The effect of sulphuric acid concentration on the electroosmotic flow was studied by varying the acid concentration from 0 to 2 M. Fig. 10a shows that the electroosmotic flow increases steadily with acid concentration. The water transport due to electroosmosis is almost doubled at 2 M acid concentration compared with that of non-doped membrane. The value of K_{Drag} however falls steadily with acid concentration, as shown in Fig. 10b. This is because a larger number of protons is now taken into account for the calculations in Eq. (17).

The variation of the electroosmotic flow with acid concentrations can be attributed to the changes in ion dispersions and the resulting net charge density distribution in the membrane. Fig. 11 shows how the H^+ (from both PEM and acid) and $SO_4{}^{2-}$ ions are distributed in the pore at 1 M acid concentration. As expected, $SO_4{}^{2-}$ ions, now present in the membrane, are repelled from the negative wall and at the same time, more protons are clustered in the close vicinity of the wall. As a result, the net charge distribution is affected which in turn modifies both the potential and the electroosmotic flow dis-

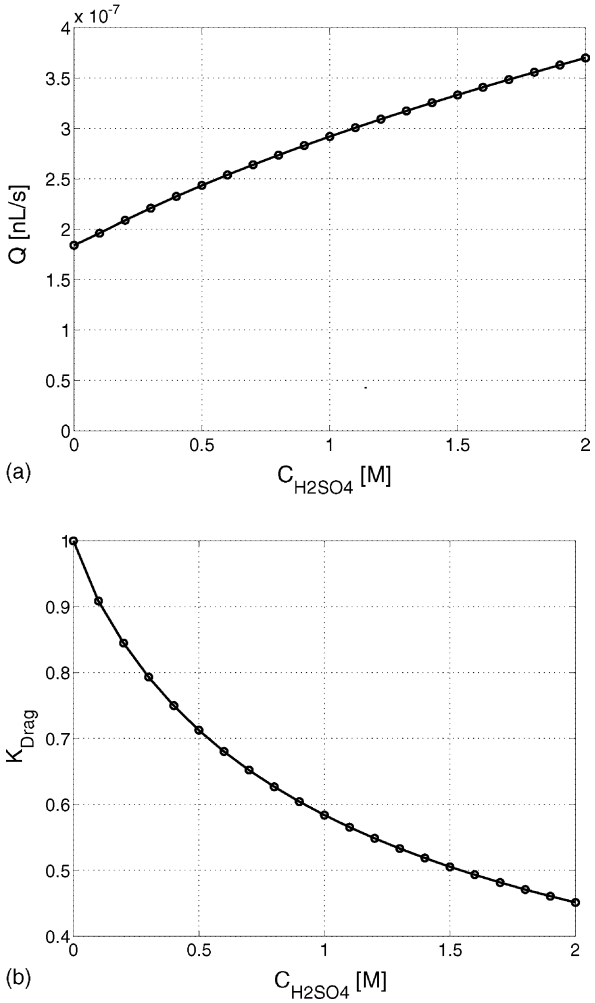

Fig. 10. (a) Electroosmotic flow and (b) electroosmotic drag coefficient as a function of sulphuric acid molarity in fully hydrated Nafion 117 membrane.

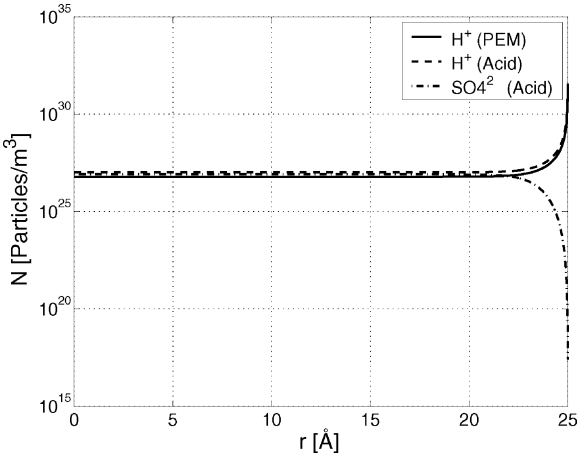

Fig. 11. Number density distributions for PEM protons and the contributions from sulphuric acid (1 M) as a function of the pore radius for fully hydrated Nafion 117 membrane with the parameter values: $\psi_w^* = -10.74$, $P^* = 0$, $M^* = -2.84$, and $E^* = -2.14$.

tributions as shown in Fig. 12. The extra protons near the wall increase the charge density there, and additional SO_4^{2-} in the centerline reduces the charge density in central regions as indicated in Fig. 12a. This causes the potential to increase sharply in the near wall region and drop in the center. Numerical results show that the wall effects are stronger at all acid concentrations as displayed in Figs. 10 and 12b,c.

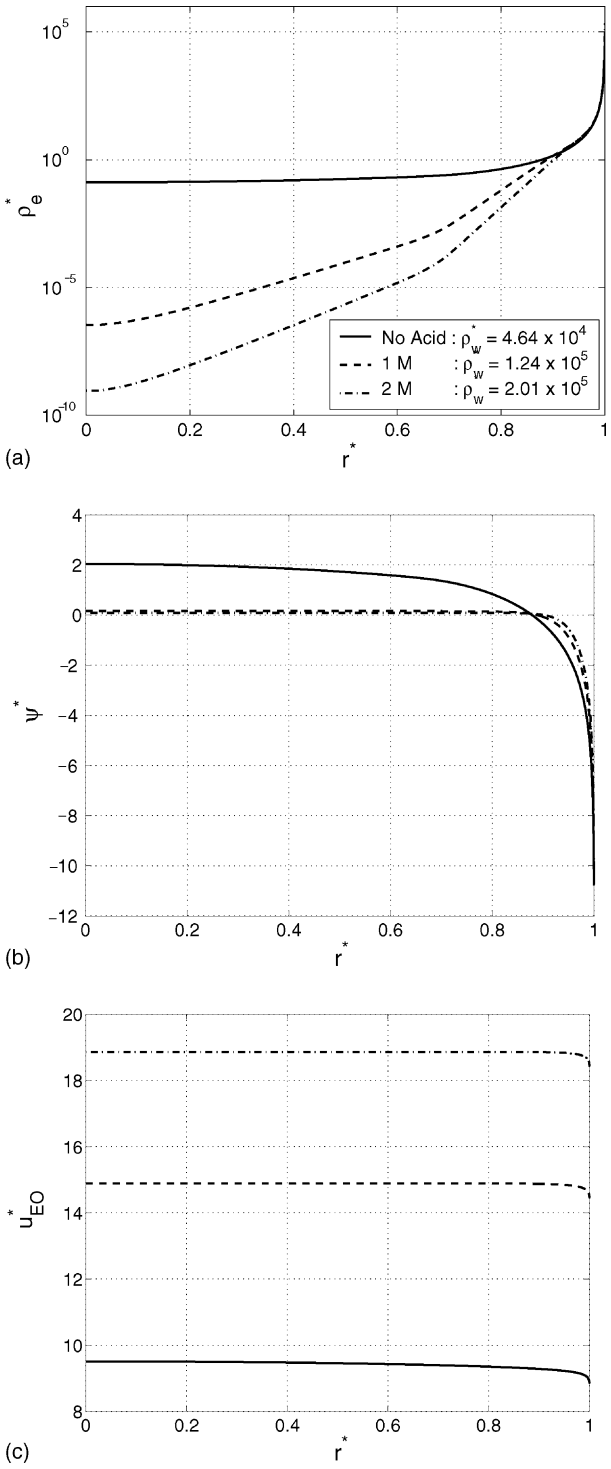

Fig. 12. Effect of sulphuric acid concentration on the distribution of (a) the charge density, (b) the potential, and (c) the resulting electroosmotic velocity through the fully hydrated Nafion 117 membrane with the parameter values: $\psi_w^* = -10.74$, $P^* = 0$, $M^* = -2.84$, and $E^* = -2.14$.

5. Conclusions

The Poisson–Boltzmann and the Navier–Stokes equations were solved numerically to determine the electroosmotic flow and the resulting electroosmotic drag coefficient in an operating PEM fuel cell. Based on the physical model and the numerical results, following conclusions can be drawn: (a) Electroosmotic flow through a single pore increases nonlinearly with the pore size. The resulting K_{Drag} increases linearly with the pore diameter. (b) The membrane thickness has a significant effect on the electroosmotic flow. At constant cell voltage, thicker membranes (e.g. Nafion 117) provide more resistance for the electroosmotic flow. However, K_{Drag} is not affected by the membrane thickness. (c) Due to the very small pore diameters (e.g. $\leq$50 Å), the pressure difference required to completely counterbalance the electroosmotic flow is very large and impractical to apply. (d) When membrane is doped with sulphuric acid, numerical results revealed that the electroosmotic flow increases steadily with the acid concentration.

Acknowledgement

This work was supported by AUTO21, the Network of Centers of Excellence, Canada.

References

[1] Th.A. Zawodzinski, S. Radzinski, R.J. Sherman, V.T. Smith, T.E. Springer, S. Gottesfeld, J. Electrochem. Soc. 140 (1993) 1041–1047.
[2] Th.A. Zawodzinski, J. Davey, J. Valerio, S. Gottesfeld, Electrochim. Acta 40 (1995) 297–302.
[3] A.B. LaConti, A.R. Fragala, J.R. Boyack, in: D.E. McIntyre, S. Srinivasan, E.G. Will (Eds.), Proceedings of the Symposium on Electrode Materials and Processes for Energy Conversion and Storage, vol. 77, 1977, p. 354.
[4] T.F. Fuller, J. Newman, J. Electrochem. Soc. 139 (1992) 1332–1339.
[5] G. Xie, T. Okada, J. Electrochem. Soc. 142 (1995) 3057–3062.
[6] X. Ren, W. Henderson, S. Gottesfeld, J. Electrochem. Soc. 144 (1997) L267–L270.
[7] K.D. Kreuer, J. Membr. Sci. 185 (2001) 29–39.
[8] C. Fang, B. Wu, X. Zhou, Electrophoresis 25 (2004) 375–380.
[9] T.D. Gierke, G.E. Munn, F.C. Wilson, J. Polym. Sci. 19 (1981) 1687–1704.
[10] R.S. Chen, J.P. Jayakody, S.G. Greenbaum, Y.S. Pak, G. Xu, J. Electrochem. Soc. 140 (1993) 889–895.
[11] S.J. Paddison, G. Bender, K.D. Kreuer, N. Nicoloso, Proceedings of the International Symposium on New Materials for Electrochemical Systems, Montreal, Canada, July 4–8, 1999.
[12] A. Lehmani, S. Durand-Vidal, P. Turq, J. Appl. Polym. Sci. 68 (1998) 503–508.
[13] B.D. Cahan, J.S. Wainwright, J. Electrochem. Soc. 140 (1993) L185–L186.

[14] S.J. Paddison, Annu. Rev. Mater. Res. 33 (2003) 289–319.
[15] B.R. Breslau, I.F. Miller, Ind. Eng. Chem. Fundam. 10 (1971) 554–565.
[16] S.W. Capeci, P.N. Pintauro, D.N. Bennion, J. Electrochem. Soc. 136 (1989) 2876–2882.
[17] P.N. Pintauro, M.W. Verbrugge, J. Membr. Sci. 44 (1989) 197–212.
[18] J.R. Bontha, P.N. Pintauro, Chem. Eng. Sci. 49 (1994) 3835–3851.
[19] M. Eikerling, A.A. Kornyshev, U.J. Stimming, Phys. Chem. B 101 (1997) 10807–10820.
[20] M. Tuckerman, K. Laasonen, M. Sprik, M. Parrinello, J. Phys. Chem. 99 (1995) 5749–5752.
[21] M. Tuckerman, K. Laasonen, M. Sprik, M. Parrinello, J. Chem. Phys. 103 (1995) 150–161.
[22] T.E. Springer, T.A. Zawodzinski, S. Gottesfeld, J. Elecetrochem. Soc. 138 (8) (1991) 2334–2342.
[23] A.W. Adamson, A.P. Gast, Physical Chemistry of Surfaces, sixth ed., John Wiley & Sons, New York, 1997.
[24] E. Barendrecht, Electrochemistry of fuel cells, in: L.J. Blomen, M. Mugerwa (Eds.), Fuel Cell Systems, Plenum Press, New York, 1993.
[25] R.F. Probstein, Physiochemical Hydrodynamics, John Wiley & Sons Inc., 1994.
[26] S.J. Paddison, R. Paul, Phys. Chem. 4 (2002) 1158–1163.
[27] R.J. Hunter, Zeta Potential in Colloid Science, Academic Press, 1981.
[28] M. Gad-el-Hak, The MEMS Handbook, CRC Press, Boca Raton, Florida, 2002.
[29] G.E. Karniadakis, A. Beskok, Microflows: Fundamentals and Simulations, Springer, 2002.
[30] P.S. Vincett, J. Colloid Interface Sci. 69 (1979) 354.
[31] D.M. Bernardi, M.W. Verbrugge, J. Electrochem. Soc. 139 (1992) 2477–2491.